Identification and characterisation of new inhibitors for the human hematopoietic prostaglandin D-2 synthase

ARTICLE *in* EUROPEAN JOURNAL OF MEDICINAL CHEMISTRY · OCTOBER 2009

Impact Factor: 3.45 · DOI: 10.1016/j.ejmech.2009.10.025 · Source: PubMed

European Journal of Medicinal Chemistry 45 (2010) 447–454

Contents lists available at ScienceDirect

European Journal of Medicinal Chemistry

journal homepage: http://www.elsevier.com/locate/ejmech

Original article

Identification and characterisation of new inhibitors for the human hematopoietic prostaglandin D_2 synthase☆

Jane E. Weber [a], Aaron J. Oakley [b], Angelika N. Christ [a], Alan G. Clark [c], John D. Hayes [d], Rhonda Hall [a], David A. Hume [e], Philip G. Board [f], Mark L. Smythe [a], Jack U. Flanagan [a,*]

[a] The University of Queensland, Institute for Molecular Bioscience, Building 80, St Lucia, Queensland 4072, Australia
[b] Research School of Chemistry, Australian National University, Canberra, ACT 2601, Australia
[c] School of Biological Sciences, Victoria University of Wellington, Wellington, New Zealand
[d] Biomedical Research Centre, Ninewells Hospital and Medical School, University of Dundee, Dundee DD1 9SY, Scotland, United Kingdom
[e] The Roslin Institute and Royal (Dick) School of Veterinary Studies, University of Edinburgh, Roslin EH25 9PS, Scotland, United Kingdom
[f] John Curtin School of Medical Research, Australian National University, Canberra, ACT 2601, Australia

ARTICLE INFO

Article history:
Received 23 February 2009
Received in revised form
18 July 2009
Accepted 15 October 2009
Available online 23 October 2009

Keywords:
Prostaglandin synthase
Docking
Structure
Inhibition
Glutathione transferase

ABSTRACT

Prostaglandin D_2 synthesised by the hematopoietic prostaglandin D_2 synthase has a pro-inflammatory effect in allergic asthma, regulating many hallmark characteristics of the disease. Here we describe identification of hematopoietic prostaglandin D_2 synthase inhibitors including cibacron blue, bromosulfophthalein and ethacrynic acid. Expansion around the drug-like ethacrynic acid identified a novel inhibitor, nocodazole, and a fragment representing its aromatic core. Nocodazole binding was further characterised by docking calculations in combination with conformational strain analysis. The benzyl thiophene core was predicted to be buried in the active site, binding in the putative prostaglandin binding site, and a likely hydrogen bond donor site identified. X-ray crystallographic studies supported the predicted binding mode.

1. Introduction

Prostaglandins (PG) are a family of structurally related eicosanoids that have regulatory roles in normal physiological as well as pathological contexts [1]. The bioactive prostanoid species PGD_2, PGE_2, PGF_2, PGI_2 and thromboxane A_2 are synthesised by specific synthases that function downstream of the cyclooxygenase enzymes [2].

PGD_2 is active in both the central nervous system and peripheral tissues, with roles in body temperature regulation, sleep wake regulation, relaxation of smooth muscle, tactile pain response, bronchoconstriction and inflammation. In mouse models of asthma and allergic disease, the prostanoid has a substantial pro-inflammatory effect, regulating many hallmark characteristics including eosinophilia, airways hyperreactivity, mucus production and Th2 cytokine levels [3–5]. Moreover, inhibition of PGD_2 synthesis as well as PGD_2 signaling blockade had a suppressive effect on neuroinflammation in mouse models of Krabbe's disease [6]. In contrast to these pro-inflammatory effects, PGD_2 and its cyclopentenone PG derivatives also have anti-inflammatory properties, with functions in inflammation resolution [7]. These studies highlight a possible therapeutic advantage in targeting the synthesis of specific prostanoids in conditions where they are pathogenic. This strategy may potentially avoid adverse effects associated with cyclooxygenase inhibitors [8] and prostacyclin loss [9].

Isomerisation of the cyclooxygenase product, PGH_2, to PGD_2 is performed by two genetically distinct PGD_2 synthase (PGDS) enzymes, brain-type-PGDS and hematopoietic-PGDS ([10,11] for reviews). The former is a member of the lipocalin superfamily, termed L-PGDS, while the latter, termed H-PGDS, is the only vertebrate member of the glutathione transferase (GST) sigma class, and requires glutathione (GSH) to perform the isomerisation reaction. Other members of the sigma class include GSTs from squid [12] and chicken [13], a cephalopod lens S-crystallin [14], and a PGD_2 synthase

Abbreviations: PG, Prostaglandin; H-PGDS, Hematopoietic prostaglandin D2 synthase; L-PGDS, Lipocalin-type prostaglandin D_2 synthase; GST, Glutathione transferase; GSH, Glutathione; H-site, Hydrophobic site; CDNB, 1 Chloro 2,4 dinitrobenzene; DMSO, Dimethyl sulfoxide.

☆ Crystallographic coordinates and structure factor amplitudes for all data sets have been deposited in the Protein Data Bank (PDB, accession code 3EE2).

* Corresponding author. Auckland Cancer Society Research Centre, Building 504, University of Auckland, Grafton, Auckland 1000, New Zealand. Tel.: +64 9 373 7599 ext 86155; fax: +64 9 373 7571.
E-mail address: j.flanagan@auckland.ac.nz (J.U. Flanagan).

0223-5234/$ – see front matter © 2009 Elsevier Masson SAS. All rights reserved.
doi:10.1016/j.ejmech.2009.10.025

from the parasite *Onchocerca volvulus* [15]. The divergence in biochemical activity and likely *in vivo* function exhibited by the sigma class GSTs is also reflected in the differences in tissue distribution. The highest levels of expression for the mammalian H-PGDS include the spleen and bone marrow [16], while the chicken GST isoform is expressed in the liver, kidney and intestine [16], and the squid GST transcript was found predominantly in the digestive gland [14]. Moreover, as mammalian L-PGDS expression appears to be mostly restricted to the central nervous system, testis and heart [11], PGD_2 synthesis in peripheral tissues is likely to be through the H-PGDS GSH dependent mechanism.

The GSTs are a family of detoxifying enzymes that can catalyse the conjugation of glutathione (GSH) to many compounds bearing electrophilic functional groups [17]. The sigma class enzymes exist as cytosolic homodimers, and have a similar tertiary structure and active site topology, despite low sequence identity, to the other classes [18]. The monomer can be divided into two domains, with the active site existing at the domain interface. The mixed α/β N-terminal domain contains the GSH binding site (G site), while the all helical C-terminal domain contributes to the PGH_2 binding site/hydrophobic substrate binding site (H-site) [19,20]. A key feature of the conjugation reaction catalysed by GSTs is the enzymes ability to activate GSH, forming and stabilizing the more reactive thiolate anion. In both the cephalopod and mammalian enzyme, an N-terminal Tyr hydroxyl is involved in the process [12,20].

The compound, HQL-79 (Fig. 1), was recently characterised as a specific inhibitor of human H-PGDS [21], and exhibited a therapeutic effect when used in animal models of allergic disease [22,23] and neuroinflammation [6]. The X-ray crystal structure of H-PGDS in complex with HQL-79 and GSH was also determined, and identified the inhibitor binding site as the putative PGH_2 binding site/H-site. The inhibitor exposed a cryptic binding site required to accommodate its di-phenyl moiety while mutagenesis data indicated an interaction between the tetrazole and residues Lys-112 and Lys-198 on the surface of the protein [21,24]. Moreover, a fragment based drug design approach identified a number of new inhibitors that bind within the active site cavity without inducing a conformational change [25].

In this study we have screened a diverse selection of broad acting GST inhibitors and related compounds, expanding the range of compounds known to inhibit H-PGDS. Here we present the biochemical and structural characterisation of nocodazole, a novel inhibitor of H-PGDS.

2. Experimental

2.1. Materials

Glutathione, 1-chloro-2,4-dinitrobenzene, cibacron blue 3G-A, indomethacin, nocodazole, oxfendazole, diclofenac, zomepirac and isoxicam were purchased from Sigma-Aldrich Pty Ltd (St Louis, MO, USA). BTB14338, HTS03989 and JFD03900 were purchased from AcrosOrganics (Geel, Belgium). Ethacrynic acid, sulfasalazine and sulfobromophthalein were purchased from MP Biomedicals (Irvine, CA, USA). HQL-79, licofelone, ramatroban and BW245C were obtained from Cayman Chemical (Ann Arbor, MI, USA). NSC4502, NSC51248 and NSC241106 were obtained from the Developmental Therapeutics Program, National Cancer Institute, NIH. AZ10535138 and tienilic acid were a gift from Astra Zeneca UK Ltd. A GSTPrep FF 16/10 glutathione agarose column

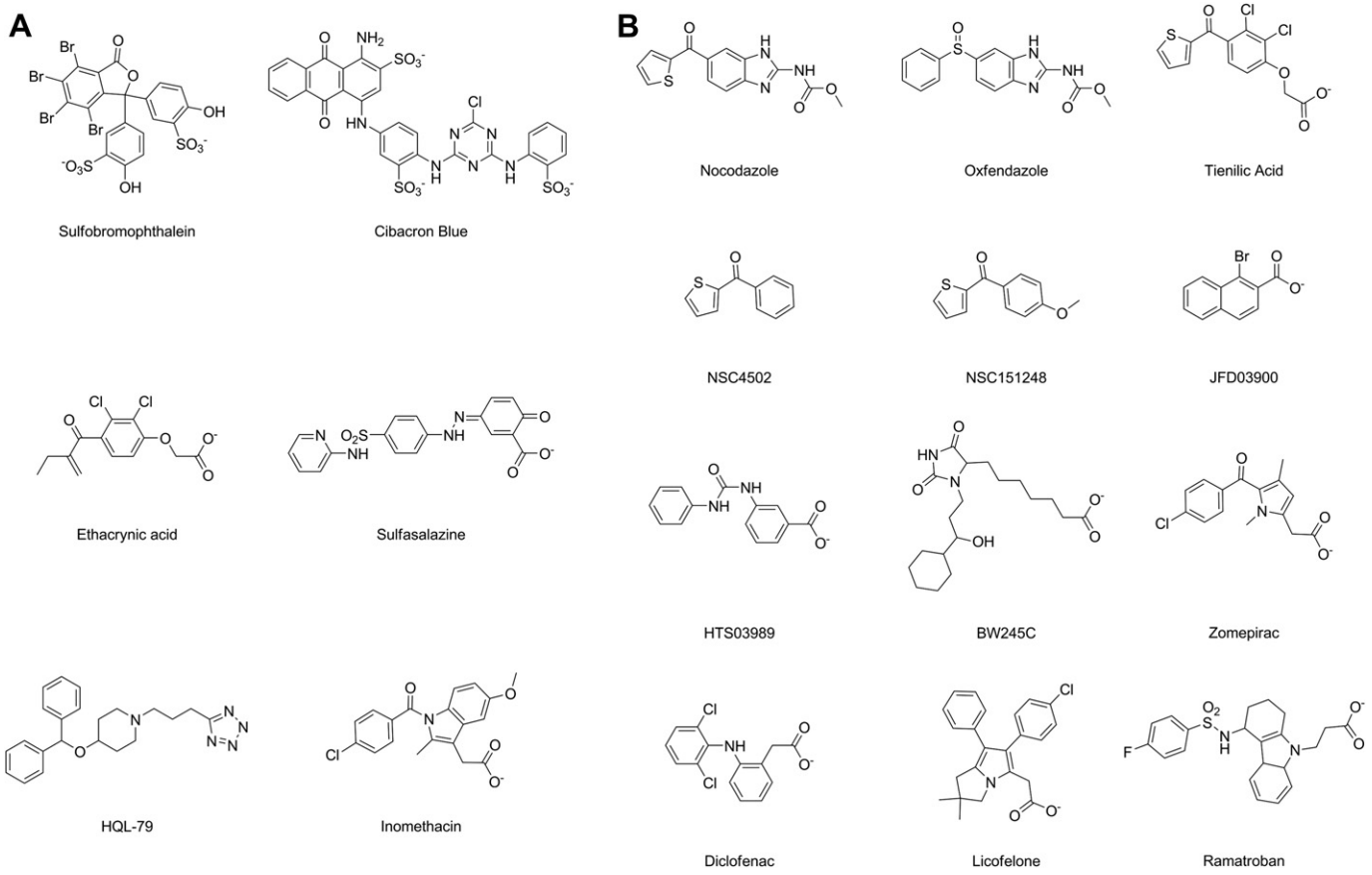

Fig. 1. A and B. Chemical structures of the selected GST inhibitors used in this study.

was purchased from GE Healthcare. Compounds were purchased from Chembridge (San Diego, CA), ABCR (Karlsruhe, Germany), Specs (Delft, The Netherlands), Alfa Aesar (Lancashire, UK), Sigma-Aldrich, Combi-Blocks (San Diego, CA) and Ryan Scientific (Mt. Pleasant, SC).

2.2. Protein expression and purification

H-PGDS was expressed and purified as described previously [16]. Briefly, H-PGDS was expressed in *Escherichia coli* strain BL21 DE3 transformed with the pET17b H-PGDS expression construct, grown overnight at 37 °C in 250 ml of Luria-Bertani medium supplemented with 100 μg/ml ampicillin. After 24 h, without induction, bacteria were harvested by centrifugation at 5000 g for 20 min at 4 °C; cell pellets were kept at −70 °C until required. Cells were resuspended in 25 ml of ice-cold phosphate buffered saline (PBS), pH 7.4, containing 1 mM DTT, 0.5% Triton X-100 and EDTA-free protease inhibitor tablets (Roche), and incubated with rotation for 30 min at 4 °C. Cells were then lysed by sonication at 90–100 W over 3 × 1 min intervals, while incubated on ice; the lysate clarified by centrifugation at 18,000*g* for 10 min at 4 °C. The supernatant was then applied to a GSTPrep FF 16/10 column pre-equilibrated with PBS, pH 7.4, and 1 mM DTT, at 0.4 ml/min using an AKTA explorer 100 (GE Healthcare), then washed with 5 column volumes of the same buffer at 1 ml/min. Bound H-PGDS was eluted in 5 column volumes of 15 mM reduced glutathione in 50 mM Tris, pH 9.0, at 0.5 ml/min, and dialysed against 100 volumes of 5 mM TrisCl, pH 8.0. The protein was concentrated to 20 mg/ml, as determined by the method of Bradford [26] using an Amicon Ultra-4 centrifugal filter device (Millipore) following manufacturers recommendations. Glycerol was added to a final concentration of 10% (v/v) prior to storage at −20 °C.

2.3. Enzyme assays

The H-PGDS catalysed conjugation of GSH and CDNB was used as the biochemical assay for enzyme inhibition. Reactions were performed in 96 well plate format, and product formation was followed at A340 nm over a 10 min interval at 25 °C using a POWERWAVE XS microplate scanning spectrophotometer (Bio-Tek Instruments). Reactions were performed in 0.1 M Tris HCl, pH 8.0 containing 2 mM $MgCl_2$, 1 mM CDNB, 2 mM GSH, 2.5 ng/μl purified H-PGDS and 10% (v/v) ethanol in a 200 μl reaction volume. IC_{50} values were calculated from rates of conjugation activity determined at eight concentration points bracketing the IC_{50}, where compound solubility allowed, and were corrected for background activity at the same solvent concentrations. The assay tolerance towards additional solvent of different types was tested up to 12.5% v/v for ethanol, methanol and DMSO. Final inhibitor solvent conditions where selected that gave less than 10% loss of enzyme activity in the system. The exceptions were nocodazole, oxfendazole, indomethacin, NSC151248 and AZ10535138, where, due to their low inhibitory activity and solubility, solvent conditions giving up to a 20% loss in enzyme activity were required to retrieve inhibition data. Non-linear regression analysis and IC_{50} calculations were performed using GraphPad Prism version 4.0c. Inhibition data at 50 uM ($I_{[50]}$) were also obtained as IC_{50} values could not be determined for all compounds.

2.4. Crystallization and data collection

Crystals were grown by the vapor-diffusion hanging drop method. The reservoir was composed of 25% PEG 6000, 25 mM $MgCl_2$, 100 mM Tris HCl pH7.5 and 1% (v/v) dioxane. Because of its low solubility, solid nocodazole crystals were placed in the drop, allowing the compound to enter the crystal by diffusion through the crystallization mixture. Prior to data collection, crystals were transferred to artificial mother-liquor identical in composition to the well solution with the addition of 20% (v/v) glycerol. Crystals were transferred using nylon loops into a cryostream at 100 K. X-ray data were collected on SBC-CAT beamline 19ID at the Advanced Photon Source using an ADSC Quantum-315 detector. Images were processed and reflection data scaled using the HKL package [27]. The structure was solved by molecular replacement in MOLREP [28]. A H-PGDS monomer taken from PDB structure 2CVD with ligands and water molecules removed was used as the search model. CCP4 and O were used for refinement and model building. The spacegroup and unit cell dimensions were consistent with an asymmetric unit containing a dimer ($V_m = 2.32$ Å^3/Da). Molecular replacement by MOLREP was successful using a radius of integration of 26Å. The rotation function (RF) revealed two peaks (RF/σ = 8.74 and 7.20) that were twice as high as the lower ranked peaks. The translation function (TF) for the highest RF peak revealed a solution (TF/σ = 15.26). With this solution fixed a translation function solution was found using the second highest RF peak (TF/σ = 64.60). Refinement commenced with the two solutions. The initial R-factor (38.88%) and R-free (38.29%) improved to 25.90% and 32.82% after 10 cycles of maximum-likelihood weighted refinement in REFMAC [29]. Four cycles of structure building in O [30] followed by refinement in REFMAC were performed during which water molecules, and a magnesium ion were built into the model. At the last cycle, nocodazole and GSH were included into the model.

2.5. Docking calculations

Ligand protein interactions were modelled by docking calculations using the program GOLDv3.0.1. Default Genetic Algorithm parameters were used, along with the Chemscore fitness function. Docking calculations were performed using the pdb entries 1IYH and 2CVD, which represent the enzyme in complex with GSH only, and in complex with both GSH and HQL-79 respectively; water and non-GSH ligands were removed. A 20 Å cavity centred on the Trp-114 Cα in subunit C and subunit D of 1IYH and 2CVD respectively was used as the docking sites. GSH was maintained in the active site and its cysteinyl thiol was either maintained as the neutral thiol, or modelled as the negatively charged thiolate species using the O.co2 atom type. As the bioactive conformation of the tested ligands is unknown, a 10 conformer library was constructed for each active compound using OMEGA2 (Openeyes) with cutoff parameters of RMS = 1.0 Å and an energy window of 10 kcal/mol. The library was docked into each active site conformation once, and the conformer with the highest Chemscore value and lowest calculated energy was selected and docked a further 10 times. All carboxylic acid moieties and the tetrazole group of HQL-79 were maintained in their deprotonated state.

2.6. Conformational strain analysis

Conformational strain was defined as the difference in energy and the RMS deviation between a bound conformation predicted by docking calculations, and its closest local minimum in the absence of protein [31,32]. Minimisation was performed using the MINIMIZE module of SYBYL7.3 with the MMFF94s force field and MMFF94 charge assignment. A distance dependent dielectric function with a dielectric constant set at 2.0 and minimal periodic boundary conditions were used. A protocol of 2000 iterations of steepest descents followed by conjugate gradients was used.

Table 1
Inhibition of human H-PGDS by selected GST inhibitors.

Compound	$I_{[50]}$	IC_{50} (μM)	Solvent (%)
Sulfobromophthalein	66.9 ± 2.3	27.0 ± 1.1	–
Cibacron Blue 3Ga	100	0.2 ± 0.001	–
Ethacrynic acid	25.3 ± 0.9	122.3 ± 1.2	EtOH (10)
HQL-79	100	1.8 ± 0.001	MeOH (10)
Sulfasalazine	0	N.D.	–
Indomethacin	0	N.D.	DMSO (10)

IC_{50} values were calculated from triplicate experiments, and are presented as IC_{50} ± Standard Error of the Mean.
$I_{[50]}$ is percent inhibition at 50 μM, and is presented as the Mean ± Standard Deviation of triplicate experiments.
N.D. not determined.
DMSO, dimethylsulfoxide; EtOH, ethanol; MeOH, methanol; where solvent is not stated, compounds were prepared in 0.1 M Tris HCl, pH 8.0 containing 2 mM $MgCl_2$.

3. Results and discussion

3.1. Biochemical characterisation of potential inhibitors

As little is known about the range of molecules that interact with the human H-PGDS active site, a number of compounds that inhibit a broad range of GSTs were selected (Fig. 1A) and screened for inhibition of the enzyme catalysed CDNB GSH conjugation reaction; the results are presented in Table 1. The known H-PGDS inhibitor HQL-79 along with the dye Cibacron Blue 3Ga, were the most potent inhibitors tested, while ethacrynic acid, a well characterised inhibitor and substrate of GSTs had a very weak interaction (IC_{50} of 122 μM). This compound represents a drug-like molecule different to that of HQL-79 [21] and other inhibitors recently identified [25], yet possesses a reactive Michael acceptor capable of conjugating with GSH and possibly protein, thus, we sought to find related compounds without this group. By performing a 2D-similarity search of an in-house database using the UNITY module of the SYBYL modelling package (Tripos, St Louis), compounds possessing a benzyl-keto-thiophene core including Tienilic acid were identified and tested (Fig. 1B, Table 2). The set was further expanded through the selection of non-steroidal anti-inflammatory drugs and ligands of the PGD_2 receptors DP1 and CRTH2 [33] (Fig. 1B); the results are presented in Table 2. These data show that H-PGDS, like other GSTs, recognises a broad ligand range, and that the absence of inhibitory effect for many tested compounds indicates a preference for particular ligands. This preference is best illustrated by comparison of nocodazole, NSC4502, tienilic acid and oxfendazole. While the inhibitory activity observed for NSC4502 and nocodazole showed that the aromatic core shared with tienilic acid can inhibit enzyme function, clearly the presence of additional Cl atoms of tienilic acid or its carboxylic acid have a negative effect on ligand binding. Moreover, the poor inhibition exhibited by oxfendazole suggests that the topology of the core may also influence ligand binding. Furthermore, the additional features present in nocodazole do not enhance the inhibitory activity of NSC4502 ($I_{[50]}$ 43% vs 78% respectively). We next sought to characterise ligand binding by molecular docking.

Table 2
Inhibition of human H-PGDS by an expanded range compounds possessing at least one aromatic and one negatively charged centre.

Compound	$I_{[50]}$	IC_{50} (μM)	Solvent (%)
Nocodazole	42.6 ± 6.4	≈65	DMSO (5)
Oxfendazole	0	>300	DMSO (5)
Tienilic Acid	0	N.D.	–
NSC4502	78.2 ± 0.4	9.2 ± 1.3	DMSO (3)
NSC151248	41.8 ± 7.8	105 ± 2.8	DMSO (7)
JFD03900	5.1 ± 3.4	N.D	DMSO (1)
HTS03989	8.6 ± 0.3	N.D	DMSO (1)
BW245C	17.0 ± 2.6	N.D	EtOH (5)
Zomepirac	0	N.D	DMSO (4)
Diclofenac	0	N.D	–
Licofelone	0	N.D	DMSO (5)
Ramatroban	0	N.D	EtOH (4)

IC_{50} values were calculated from triplicate experiments, and are presented as IC_{50} ± Standard Error of the Mean. The IC_{50} value for nocodazole is an approximation estimated from fitting an incomplete dataset due to limited compound solubility.
$I_{[50]}$ is percent inhibition at 50 μM, and are presented as the Mean ± Standard Deviation of triplicate experiments.
N.D not determined.
DMSO, dimethylsulfoxide; EtOH, ethanol; where solvent is not stated, compounds were prepared in 0.1 M Tris HCl, pH 8.0 containing 2 mM $MgCl_2$.

3.2. Binding site prediction

Comparison of the crystal structures for the GSH only (pdb 1IYH), and GSH HQL-79 bound enzyme (pdb 2CVD) revealed the presence of a cryptic pocket that binds a phenyl moiety of the inhibitor, and is defined by residues (Met-99, Phe-102, Trp-104, Tyr-152 and Thr-159). As the inhibitors identified in this study are structurally and physicochemically un-related to HQL-79, the active site conformation they recognise is not clear. We applied a combination of docking calculations and conformational strain analysis to predict the most likely protein conformation and binding mode using nocodazole as a representative for the set of benzyl-keto-thiophene containing compounds tested in this study.

The applicability of the docking program GOLD, to the prediction of ligand binding modes in the H-PGDS active site was assessed by its ability to calculate the binding mode of HQL-79 observed in the pdb entry 2CVD, and was best achieved using the Chemscore scoring function. As there is evidence to suggest that mammalian H-PGDS can, like other GSTs, activate GSH, docking calculations were performed in both the absence and presence of a negatively charged anion representing the thiol and thiolate species respectively. Notably, an effect was observed with the lower ranked poses in the presence of the model anion, where the negative charge appeared to limit incorrect positioning of the benzyl moieties, thus the model thiolate was maintained in all docking calculations. The H-PGDS active site transitions from a clearly defined inner cavity through to a broad, peripheral solvent exposed component that in the case of HQL-79 is occupied by a benzyl ring and the tetrazol moitey respectively. Analysis of this complex illustrated that the tetrazol made few direct contacts with the protein and had a greater degree of mobility [21], this was also reflected in the variance of the tetrazol position in our docking studies.

In a comparison between docking single and multiple nocodazole conformations, we noted that a range of Chemscore values were obtained with different starting conformations. The highest scoring conformer was subsequently selected for further, more rigorous docking studies. Visual inspection of the five best solutions, as judged by Chemscore, illustrated that nocodazole occupied the cryptic pocket when available however, the Chemscore values (ranging from 24.67 to 28.55 and 24.59 to 26.61 in cryptic pocket presence (2CVD) and absence (1IYH) respectively) did not differentiate between the two binding sites. Where the cryptic pocket was unavailable, the best ranked modes all had good agreement in the location of the aromatic core, while divergence in the orientation of the carbamate group reduced confidence in its predicted location and active site interactions. The thiophene ring was predicted to bind in the inner cavity, in a predominantly hydrophobic pocket defined by the side chains of Arg-14 (salt linked to Asp-96), Met-99, Tyr-152, Ile-155 and Cys-156, while the ligands carbonyl group was positioned close to the side chain hydroxyl of Thr-159, implying a hydrogen bond interaction. The benzimidazole group was located centrally in the active site in an orientation where the

Table 3
Conformational strain analysis.

Structure	Chemscore	$\Delta E_{[DOCK-MIN]}$ (kcals/mol)	RMSD $_{[DOCKvMIN]}$ (Å)
Nocodazole			
cryptic pocket absence	26.49	13.63	0.28
cryptic pocket presence	26.61	36.19	0.66

Conformational strain analysis is presented for the solution with the best Chemscore value in the most populated pose. The structures 1IYH and 2CVD were used to represent the absence and presence of the cryptic binding pocket.

phenyl ring was predicted to interact with the side chains of Met-11, Gly-13, Trp-104 and Leu-199, while the imidazole ring and carbamate moiety were positioned in the less constrained peripheral site.

In contrast, on exposure of the cryptic pocket, a different binding site was predicted where the thiophene ring was positioned within the new cavity, between residues Phe-102, Trp-104, Phe-116, Leu-160 and Phe-163; the carbonyl group did not form an interaction with the Thr-159 hydroxyl. The benzimidazole group was positioned between the side chains of Trp-104 and the alkyl region of Arg14, and was not centrally located in the active site cavity, with the methylated carbamate extending out of the active site into the intersubunit cleft. Overall, the solutions for the aromatic core were not well clustered.

We hypothesised that these two different binding sites are likely to impart different conformational strain effects on the ligand, and that the active site conformation most likely to bind nocodazole would cause the least strain, thus have better steric and electrostatic complementarity [31]. An analysis of conformational strain was performed on the calculated binding modes for nocodazole in both active site conformations, and the results for the highest scoring pose are presented in Table 3. The data clearly illustrate that nocodazole is least conformationally strained when the cryptic pocket is unavailable, strongly implying that it is more likely to bind to the GSH only complex.

3.3. Binding mode characterisation

As the benzyl-keto-thiophene containing compounds represent a new inhibitory chemotype for H-PGDS, we assessed the accuracy of the docking calculations in predicting the nocodazole binding mode by x-ray crystallography; the crystallographic data for the crystal structure of H-PGDS with GSH and nocodazole bound are presented in Table 4. A crystal of the complex was obtained with a $P2_12_12_1$ space group, with a dimer located in the asymmetric unit, an arrangement not previously observed for human H-PGDS [21,34]. At 1.90 Å resolution, the electron density maps ($2mF_o$-DF_c and mF_o-DF_c) revealed excellent density for the protein, and a series of $>3.5\ \sigma$ peaks in the mF_o-DF_c difference map in the vicinity of the active site were interpreted as nocodazole and GSH. Nocodazole was observed in subunit A only, having a density that clearly described the orientation of the complete molecule (Fig. 2A). A variation in the N-terminal of α5-helix position was observed in both subunits. The structure was more comparable with the GSH only complex (pdb 1IYH) than that with HQL-79 (pdb 2CVD) with RMSDs of 0.4683 and 0.7643 Å across 394 superimposed Cα atoms of the dimer respectively.

Nocodazole was located in the putative prostaglandin binding site/GST H-site, opposite GSH. The thiophene ring was located in a pocket defined by Arg-14 (linked to Asp-96 via a salt bridge), Met-99, Tyr-152, Leu-155 and Cys-156, while the carbonyl group was within hydrogen bonding distance to the structural water, HOH150, which contacts the side chain OH group of Thr-159 and the free carboxylate group of the C-terminal residue Leu-199. The benzimidazole group was positioned centrally in the active site cavity, occupying a space between Gly-13, Trp-104, the alkyl region of the Arg-14 side chain, and the GSH thiol (Fig. 2B), while the carbamate moiety was orientated away from GSH, extending toward Lys-112 at the periphery of active site. When compared to the predicted binding modes, there was good agreement in the position of the benzyl-keto-thiophene centre (Fig. 2B), yet no calculated pose correctly positioned the carbamate tail. The side chain positions of active site residues are consistent with the GSH only complex, and the structure clearly shows that nocodazole does not access the cryptic binding site as predicted by our conformational strain analysis. This is further illustrated by comparison with the HQL-79 bound structure (Fig. 2C). Both compounds fill the main active site cavity with good overlap between the position of nocodazoles thiophene ring and a phenyl ring of HQL-79.

The structures for a number of low molecular weight H-PGDS inhibitors, each possessing at least two aromatic centres in a planar orientation were recently published [25]. Comparison of these to the nocodazole and GSH [34] only structures clearly illustrate that each compound binds to a very similar active site conformation that likely represents a more conventional binding mode than the induced fit of HQL-79 [21]. A structure based molecular alignment (Fig. 2D), illustrates that the aromatic cores of all compounds align well, with nocodazoles thiophene moiety matching the buried benzyl ring common to the other ligands, while the benzimidazole group aligns with the aromatic centres occupying the central cavity with some overlap into the solvent exposed part by the carbamate side chain. Although other compounds possessing H bond acceptor sites (pdb codes 2VCQ, 2VCW, 2VCX) interact with the same ordered water as the carbonyl linker group in nocodazole these sites do not align. Moreover, the linker carbonyl group of tranilast interacts directly with the Thr-159 side chain hydroxyl directly, and does not superimpose with that in nocodazole. Notably, the nocodazole carbamate group adopted an orientation not observed in other inhibitor complexes.

Table 4
X-ray and structure data.

Space Group	**$P2_12_12_1$**
Unit Cell (Å,°)	a = 47.22 b = 79.36 c = 107.55 α = β = γ = 90
Wavelength (Å)	0.97948
Resolution (Å)	50.0-1.90 (1.97-1.90)[a]
⟨I/σI⟩	18.56 (2.32)
R-merge (%)[b]	6.3 (64.5)
Completeness (%)	87.9 (83.6)
Unique Reflections	28391 (2644)
Average Redundancy	3.4 (3.4)
R-factor, R-free (%)[c]	18.40, 23.40
RMS Deviations From Ideal Values:	
-Bond Lengths (Å)	0.019
-Bond Angles (Degrees)	1.798
-Chiral-Center Restraints (Å^3)	0.125
Number of atoms	
-protein	3278
-GSH	20
-Nocodazole	21
-Mg^{2+}	1
-water	180
Ramachandran plot	
-Residues in most-favourable region:	93.3%
-Residues in additionally allowed region:	6.1%
-Residues in generously allowed regions:	0.6%

[a] Figures in parentheses refer to highest resolution bin.
[b] R-merge = $\Sigma_h\Sigma_i\ |I_{hi} - \langle I_h\rangle|/\Sigma_h\Sigma_i I_h$.
[c] R-factor = $\Sigma_h\ ||F_{obs}| - |F_{calc}||/\Sigma|F_{obs}|$ where F_{obs} and F_{calc} are the respectively the observed and calculated structure factors. R-free was calculated from 5% of the diffraction data not used in refinement.

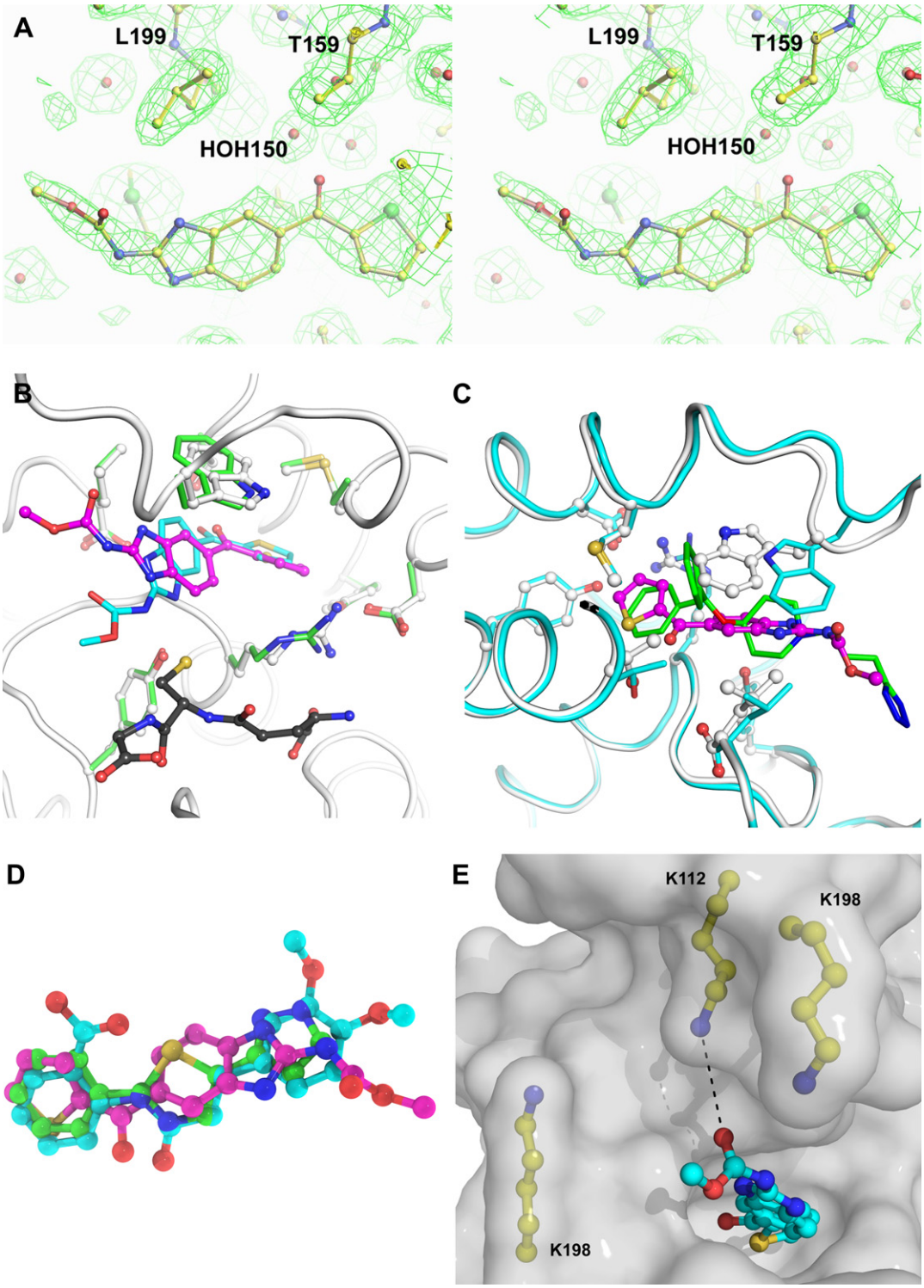

Fig. 2. (A) Stereo diagram of the nocodazole, GSH, Mg^{2+} H-PGDS structure showing fitted electron density around nocodazole. Illustrated is the hydrogen bond interaction with HOH150 located between the side chain OH of Thr159 and the free COOH group of Leu199. (B) Superimposition of the best nocodazole binding mode calculated by GOLD (cyan sticks), and that determined crystallographically (magenta ball and stick). Active site residues in the GSH H-PGDS only structure (pdb 1IYH) predicted to be involved in nocodazole binding are shown as green sticks, while the same residues in the experimentally determined nocodazole GSH H-PGDS structure are illustrated as light grey ball and stick. (C) Superimposition of the nocodazole and HQL-79 (pdb 2CVD) structures clearly indicates that nocodazole does not access the cryptic binding site required to coordinate the di-phenyl core of HQL-79. Nocodazole is shown in magenta ball and stick, and HQL-79 as green sticks. The Cα trace of the nocodazole complex is shown as a white ribbon, with key active site residues in ball and stick representation, while that of the HQL-79 complex is in cyan and key active site residues in stick representation. (D) A structure based alignment of nocodazole (magenta ball and stick) with tranilast (cyan ball and stick) and compound **13** (green ball and stick) [25]; included is HOH150. (E) Location of the nocodazole carbamate relative to Lys-112, also illustrated are Lys107 and Lys108 that form a positively charged surface cluster.

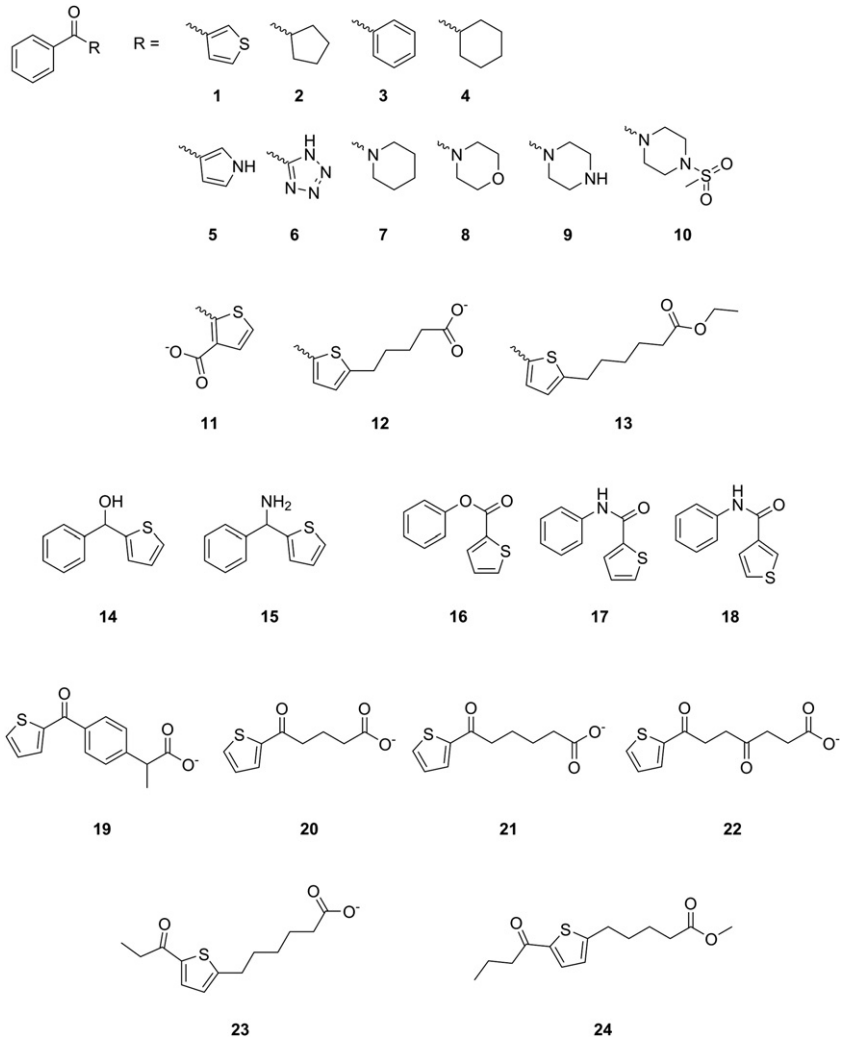

Fig. 3. Chemical structures of compounds used to probe the benzyl thiophene binding site.

We next sought to characterise more fully the interactions between the benzyl-keto-thiophene fragment and the H-PGDS active site, by probing the active site with the compounds presented in Fig. 3; the results are presented in Table 5. Reorientation of the thiophene or substitution with a cyclopentyl ring were tolerated (compounds **1** and **2**), while increasing the ring size using both aromatic and saturated systems had a dramatic negative effect on IC_{50}, and suggested a size limitation at this site (compounds **3** and **4**). A basic nitrogen was not well tolerated at this position (compound **5**), and acidic groups (compounds **6** and **11**) also had a negative effect on inhibitory activity. The nature of the hydrogen bond contact with the structurally conserved water was also explored, with compounds **14** and **15** providing a ligand hydrogen bond donor. The IC_{50} was substantially decreased supporting a hydrogen bond donor and acceptor role for the water HOH150 and ligand carbonyl group respectively. The effect of including a spacer around the carbonyl (compounds **16**, **17** and **18**) did not improve activity. Taken together, these data suggest that the benzyl-keto-thiophene binding site is predominantly hydrophobic with an accessible hydrogen bond donor site. Interestingly, a carboxylate group is tolerated on other scaffolds as seen with tranilast, where a benzoic acid located in the inner active site cavity, although the carboxylate does interact with the side chain of Arg-14 (pdb 2vd0).

3.4. Exploring the potential for a remote binding site

The proximity of nocodazoles carbamate group to Lys-112, and the presence of Lys-107 and Lys-198 around the active site entrance (albeit at 6.7 and 7.56 Å from the carbamate respectively) (Fig. 2E) suggested that a carboxylate group in this region may increase ligand affinity, a hypothesis further supported by the detrimental effect of charge swap mutations at these positions on HQL-79 binding [21]. A number of compounds possessing either a carboxylic acid or ester moiety attached to the benzyl-keto-thiophene core through an alkyl chain were identified using the ZINC web resource [35] and characterised; the compounds are illustrated in Fig. 3 and the results presented in Table 5. Most compounds characterised had a derivatised thiophene moiety that, in the nocodazole structure, is buried in the inner active site cavity. Notably, the active compounds were less potent than NSC4502 at 50 μM, indicating that the additional groups did not improve NSC4502 affinity. Overall, activity within this series of compounds does require the presence of two aromatic centres, consistent with other studies [25].

Table 5
Inhibition of human H-PGDS by NSC4502 derivatives.

Compound		$I_{[50]}$	IC_{50} (μM)
Phenyl-(3-thienyl)-methanone	1	84.1 ± 3.2	11.4 ± 1.2
Cyclopentyl-phenylketone	2	77.7 ± 1.8	16.0 ± 1.1
benzophenone	3	62.5 ± 3.0	62.2 ± 1.2
Cyclohexyl-phenylketone	4	37.9 ± 2.2	>100
3-benzoylpyrrole	5	57.4 ± 1.4	87.5 ± 1.1
Phenyl-2H-tetrazole-5-yl-methanone	6	1.4 ± 3.7	–
1-benzoyl piperidine	7	17.6 ± 3.0	>100
Morpholino-(phenyl)-methanone	8	19.0 ± 9.0	–
1-benzoyl piperazine	9	8.5 ± 1.9	>100
1-benzoyl-4-(methylsulfonyl)piperazine	10	14.6 ± 2.0	>100
NSC241106	11	0	–
CMB5190724	12	40.4 ± 3.6	117 ± 1.5
CMB5256165	13	42.5 ± 2.4	>100
Phenyl-(-2-thienyl)-methanol	14	5.6 ± 1.0	>100
1-phenyl-1-(2-thienyl)methanamine	15	4.14 ± 1.4	>100
Phenyl-thiophene-2-carboxylate	16	14.5 ± 0.9	–
N-phenyl-2-thiophene-carboxamide	17	7.2	>100
N-phenyl-3-thiophene-carboxamide	18	6.06 ± 2.4	–
AZ10535138	19	0	–
AB179670	20	14.5 ± 2.2	>100
AI-942/25034756	21	0	–
CMB6848429	22	0	–
CMB5256116	23	0	–
CMB5256095	24	0	–

IC_{50} values were calculated from triplicate experiments, and are presented as IC_{50} ± Standard Error of the Mean. $I_{[50]}$ is percent inhibition at 50 μM, and are presented as the Mean ± Standard Deviation of triplicate experiments.
N.D. not determined.
Compounds were prepared in 0.1 M Tris HCl, pH 8.0 containing 2 mM $MgCl_2$ with the exception of AZ10535138 which was used at 10% DMSO.

4. Conclusion

We have identified a diverse range of compounds that inhibit the H-PGDS glutathione conjugating activity including small, drug-like molecules as well as very high molecular weight dyes, and demonstrated that H-PGDS exhibits the broad ligand selectivity well characterised for other members of the glutathione transferase superfamily [13,36]. The enzyme nocodazole interaction was further characterised in more detail using both biophysical and computational methods, with a simple approach to conformational strain analysis correctly predicting a preferred active site conformation and the position of the benzyl thiophene core.

Importantly, nocodazole, along with the smaller benzyl thiophene fragment NSC4502 represent novel low molecular weight probes of H-PGDS, and identified a structural water within the hydrophobic inner active site cavity as a hydrogen bond donor site. A structure based alignment of nocodazole and recently identified high affinity inhibitors [25], demonstrated that thiazole and isoxazole nitrogen atoms also targeted the same site. Interestingly, the carbamate side chain of nocodazole also suggests the possibility of a remote binding site that may be exploited in design strategies.

Acknowledgements

We thank the Developmental Therapeutics Program NCI/NIH, and Dr Peter Newham (Astra Zeneca) for supplying compounds used in this study; the Australian Research Council Special Research Centre for Functional and Applied Genomics and Cooperative Research Centre for Chronic Inflammatory Disease for equipment access. This work is funded by an Australian National Health and Medical Research Council Project Grant (455949). JUF was funded by a NHMRC Howard Florey Centenary Fellowship (2004001540).

References

[1] D.L. Simmons, R.M. Botting, T. Hla, Pharmacol. Rev. 56 (2004) 387.
[2] R.J. Helliwell, L.F. Adams, M.D. Mitchell, Prostaglandins Leukot. Essent. Fatty Acids 70 (2004) 101.
[3] A. Arimura, K. Yasui, J. Kishino, F. Asanuma, H. Hasegawa, S. Kakudo, M. Ohtani, H. Arita, J Pharmacol. Exp. Ther. 298 (2001) 411.
[4] T. Matsuoka, M. Hirata, H. Tanaka, Y. Takahashi, T. Murata, K. Kabashima, Y. Sugimoto, T. Kobayashi, F. Ushikubi, Y. Aze, N. Eguchi, Y. Urade, N. Yoshida, K. Kimura, A. Mizoguchi, Y. Honda, H. Nagai, S. Narumiya, Science 287 (2000) 2013.
[5] Y. Fujitani, Y. Kanaoka, K. Aritake, N. Uodome, K. Okazaki-Hatake, Y. Urade, J. Immunol. 168 (2002) 443.
[6] I. Mohri, M. Taniike, H. Taniguchi, T. Kanekiyo, K. Aritake, T. Inui, N. Fukumoto, N. Eguchi, A. Kushi, H. Sasai, Y. Kanaoka, K. Ozono, S. Narumiya, K. Suzuki, Y. Urade, J. Neurosci. 26 (2006) 4383.
[7] S.G. Trivedi, J. Newson, R. Rajakariar, T.S. Jacques, R. Hannon, Y. Kanaoka, N. Eguchi, P. Colville-Nash, D.W. Gilroy, Proc. Natl. Acad. Sci. U S A 103 (2006) 5179.
[8] G.A. FitzGerald, Trends Pharmacol. Sci. 28 (2007) 303.
[9] H. Francois, K. Athirakul, D. Howell, R. Dash, L. Mao, H.S. Kim, H.A. Rockman, G.A. Fitzgerald, B.H. Koller, T.M. Coffman, Cell Metab. 2 (2005) 201.
[10] Y. Kanaoka, Y. Urade, Prostaglandins Leukot. Essent. Fatty Acids 69 (2003) 163.
[11] Y. Urade, O. Hayaishi, Biochim. Biophys. Acta. 1482 (2000) 259.
[12] X. Ji, E.C. von Rosenvinge, W.W. Johnson, S.I. Tomarev, J. Piatigorsky, R.N. Armstrong, G.L. Gilliland, Biochemistry 34 (1995) 5317.
[13] A.M. Thomson, D.J. Meyer, J.D. Hayes, Biochem. J. 333 (1998) 317.
[14] S.I. Tomarev, R.D. Zinovieva, K. Guo, J. Piatigorsky, J. Biol. Chem. 268 (1993) 4534.
[15] A. Sommer, R. Rickert, P. Fischer, H. Steinhart, R.D. Walter, E. Liebau, Infect. Immun. 71 (2003) 3603–3606.
[16] I.R. Jowsey, A.M. Thomson, J.U. Flanagan, P.R. Murdock, G.B. Moore, D.J. Meyer, G.J. Murphy, S.A. Smith, J.D. Hayes, Biochem. J. 359 (2001) 507.
[17] J.D. Hayes, J.U. Flanagan, I.R. Jowsey, Annu. Rev. Pharmacol. Toxicol. 45 (2005) 51–88.
[18] A.J. Oakley, Curr. Opin. Struct. Biol. 15 (2005) 716.
[19] Y. Kanaoka, H. Ago, E. Inagaki, T. Nanayama, M. Miyano, R. Kikuno, Y. Fujii, N. Eguchi, H. Toh, Y. Urade, O. Hayaishi, Cell. 90 (1997) 1085.
[20] E. Pinzar, M. Miyano, Y. Kanaoka, Y. Urade, O. Hayaishi, J. Biol. Chem. 275 (2000) 31239.
[21] K. Aritake, Y. Kado, T. Inoue, M. Miyano, Y. Urade, J. Biol. Chem. 281 (2006) 15277.
[22] N. Matsushita, K. Aritake, A. Takada, M. Hizue, K. Hayashi, K. Mitsui, M. Hayashi, I. Hirotsu, Y. Kimura, T. Tani, H. Nakajima, Jpn. J. Pharmacol. 78 (1998) 11.
[23] N. Matsushita, M. Hizue, K. Aritake, K. Hayashi, A. Takada, K. Mitsui, M. Hayashi, I. Hirotsu, Y. Kimura, T. Tani, H. Nakajima, Jpn. J. Pharmacol. 78 (1998) 1.
[24] E. Pinzar, Y. Kanaoka, T. Inui, N. Eguchi, Y. Urade, O. Hayaishi, Proc. Natl. Acad. Sci. U S A 97 (2000) 4903.
[25] M. Hohwy, L. Spadola, B. Lundquist, P. Hawtin, J. Dahmen, I. Groth-Clausen, E. Nilsson, S. Persdotter, K. von Wachenfeldt, R.H. Folmer, K. Edman, J. Med. Chem. 51 (2008) 2178.
[26] M.M. Bradford, Anal. Biochem. 72 (1976) 248.
[27] Z.a.M.W. Otwinowski, Methods in Enzymology 276 (1997) 307.
[28] A.a.T. Vagin, J. Appl. Cryst. 30 (1997) 1022.
[29] M. Winn, M. Isupov, G.N. Murshudov, Acta Crystallogr. D57 (2001) 122.
[30] T.A. Jones, J.Y. Zou, S.W. Cowan, M. Kjeldgaard, Acta Crystallogr. A47 (1991) 110.
[31] R.D. Head, M.L. Smythe, T.I. Oprea, C.L. Waller, S.M. Green, G.R. Marshall, JACS 118 (1996) 3959.
[32] E. Perola, P.S. Charifson, J. Med. Chem. 47 (2004) 2499.
[33] A.N. Hata, T.P. Lybrand, L.J. Marnett, R.M. Breyer, Mol. Pharmacol. 67 (2005) 640.
[34] T. Inoue, D. Irikura, N. Okazaki, S. Kinugasa, H. Matsumura, N. Uodome, M. Yamamoto, T. Kumasaka, M. Miyano, Y. Kai, Y. Urade, Nat. Struct. Biol. 10 (2003) 291.
[35] J.J. Irwin, B.K. Shoichet, J. Chem. Inf. Model. 45 (2005) 177.
[36] B. Mannervik, U.H. Danielson, CRC Crit. Rev. Biochem. 23 (1988) 283.